Original Research

Utility of Noncontrast-enhanced Time-Resolved Four-Dimensional MR Angiography with a Vessel-selective Technique for Intracranial Arteriovenous Malformations

ABSTRACT

Purpose: To evaluate the utility of a vessel-selective four-dimensional (4D) magnetic resonance angiography (MRA) technique for the evaluation of intracranial arteriovenous malformations (AVMs).

Materials and Methods: Twelve AVM patients were evaluated retrospectively. Time-of-flight (TOF) MRA, non-vessel-selective 4D-MRA (NS-4D-MRA) and vessel-selective 4D-MRA (VS-4D-MRA) were performed using a 3-tesla MR unit in all patients, and used to identify feeding arteries and draining veins and measure nidus size. The diagnostic accuracy of the three techniques was compared using digital subtraction angiography (DSA). If a multi-feeder was observed, the percentage of blood flow of each feeding artery to the entire nidus was evaluated, and compared to the DSA findings using the ‘error value’, defined as the degree of overestimation of the blood flow. All imaging findings were assessed by two neuroradiologists.

Results: In both raters, the detectability of feeding arteries by VS-4D-MRA (12 and 11 patients) was significantly higher than those of TOF-MRA (7 and 6 patients) and NS-4D-MRA (8 and 7 patients) ($p<0.016$, respectively). The detectability of drainer veins by TOF-MRA (10 and 10 patients) was significantly higher than that of

VS-4D-MRA (7 and 6 patients). In the percentage of the blood flow of each feed artery to the entire nidus, the DSA findings (error value; 27.1 ± 5.7) indicated overestimations of the blood flow compared to the VS-4D-MRA (error value; 7.1 ± 3.9) ($p<0.001$).

Conclusions: VS-4D-MRA was shown to be a useful technique for the evaluation of intracranial AVMs, especially for detecting feed arteries and estimating details of the nidus structure.

Keywords: arteriovenous malformation, arterial spin labeling, 4D-MRA, vessel-selective technique

Introduction

Cerebral arteriovenous malformation (AVM), a congenital disorder observed in young individuals, can be a cause of subarachnoid hemorrhage, brain hemorrhage, or a hemorrhagic stroke (1,2). AVMs consist of abnormal blood vessels with intracerebral direct connections between cerebral arteries and veins, without a normal capillary bed. Detailed information including the anatomic and hemodynamic characteristics of individual cases of AVM (e.g., the size, feeding arteries, and draining vein) is required for the appropriate assessment of this disease (3–5).

Digital subtraction angiography (DSA) is considered the gold standard for the evaluations of AVMs. However, the DSA procedure is invasive and may thus result in a number of complications, such as stroke, hematoma near the puncture spot, or aortic dissection (6,7). In addition, a power injector is usually used for the contrast medium injection for DSA, and this may cause different findings compared to normal physiological hemodynamics because of the strong positive pressure of the contrast medium.

As an alternative method for the noninvasive assessment of AVMs, magnetic resonance angiography (MRA) has been proposed (8). Three-dimensional time-of-flight

(TOF) MRA is the most common technique. However, 3D TOF-MRA visualizes a static phase of blood vessels, preventing an accurate differentiation between the arterial and venous phases, and it does not demonstrate hemodynamic information of AVMs. Contrast-enhanced time-resolved MRA techniques have been developed for the assessment of cerebral AVMs (9,10), but this method also involves the rapid injection of contrast agent, moreover, the temporal resolution of this technique (approx. 1 sec) is not considered sufficient for the separate depiction of the feeding artery, nidus and drainer vein in AVMs.

In recent years, a technique for evaluating AVMs that uses noncontrast-enhanced four-dimensional (4D) MRA with arterial spin labeling has been described (11–13). This technique can simultaneously visualize the vascular morphology and dynamic blood flow of a feeding artery, the nidus, and the draining veins, without the administration of a contrast agent. In addition, 4D-MRA can visualize the dynamic flow with vessel selectivity by using the location of a free labeling slab placed on the targeted vessel (14). This vessel-selective arterial dynamic information is important and useful for assessing AVMs.

Our aim in the present study was to assess the utility of the vessel-selective 4D-MRA (VS-4D-MRA) technique for the evaluation of intracranial AVMs.

Materials and Methods

Patients

This retrospective study was approved by our institutional review board, and informed consent was waived. We retrospectively evaluated the cases of 12 patients who were examined in our hospital between October 2012 and November 2015 with the following inclusion criteria: (1) a cerebral AVM confirmed by DSA, (2) the AVM was newly diagnosed and untreated in the past, and (3) the DSA examination was performed within 1 month after a magnetic resonance (MR) examination. Patients were excluded for whom (1) one or more of the three scans, TOF-MR, non-vessel-selective 4D-MRA (NS-4D-MRA) and VS-4D-MRA was not performed in the MR examination or (2) the right internal carotid artery (Rt. IC), left internal carotid artery (Lt. IC) or dominant side of the vertebral artery was omitted from the DSA investigations. The patients were eight males and four females (mean age 32.3 years; age range 5–69 years). The interval between the DSA and the 4D-MRA for each patient ranged from 1 to 28 days (mean 5.2 days). In all 12 patients, follow-up MR examination was performed within 1 week after DSA; it was confirmed that no large changes such as feeder occlusion had occurred between the 4D-MRA and DSA examinations by confirming that there was no change

of imaging findings in the nidus and proximal arteries/veins between the first and follow-up MR examinations.

Imaging techniques

All patients received 4 types of scans: 1) TOF-MRA, 2) NS-4D-MRA, 3) VS-4D-MRA and 4) DSA. In 12 patients, the series of VS-4D-MRA included three arterial territory images (total 36 images), whereas the other 3 scans (NS-4D-MRA, TOF-MRA and DSA) comprised only 1 image per patient (12 images each).

MRI technique

For 4D-MRA analysis, we analyzed a series of 36 images obtained by VS-4D-MRA and 12 by NS-4D-MRA. All MR scanning was performed using a 3.0-Tesla unit (Achieva TX; Philips Healthcare, Best, the Netherlands) with an eight-channel head coil. A tagging scheme of echo planar imaging and signal targeting with alternating radiofrequency (EPI-STAR) was used for the labeling of arterial blood in neck lesions. For the image acquisition, look-locker sampling with a 200-ms post-labeling delay and phase intervals of 212 ms was used with the turbo-field-echo echo-planar imaging (TFEPI) readout technique. The imaging parameters of the NS-4D-MRA were as follows: TR 13 ms, TE 5 ms, TFE factor 13, EPI factor 5, flip

angle 10°, field of view (FOV) 230 mm, matrix 192 × 192, slice thickness 1.4 mm (slice pitch 0.7 mm), 150 slices (slab thickness 105 mm), scan time 5’49. The imaging parameters of the VS-4D-MRA were as follows: TR 13 ms, TE 5 ms, TFE factor 13, EPI factor 5, flip angle 10°, FOV 230 mm, matrix 192 × 192 (256 × 256 reconstruction), thickness 1.8 mm (slice pitch 0.9 mm), 120 slices (slab thickness 108 mm), scan time 3’51. In both the NS- and VS-4D-MRA, a total of eight phases’ (labeling after 200, 412, 624, 836, 1048, 1260, 1472, and 1684 ms) dynamic images were obtained (Fig. 1). For the NS-4D-MRA, a 30-mm-thick labeling slab was set just under the imaging plane. For the vessel-selective tagging, the right common carotid artery, left common carotid artery, and bilateral vertebral artery were selectively labeled using a spatial free labeling slab to selectively visualize the territory of the Rt. IC, Lt. IC and vertebro-basilar artery (VBA) respectively, by carefully avoiding other non-selected vessels in the tagging area. Just after the labeling, the regional saturation pulse was achieved to saturate the arterial flow signal from the lower stream, such as that from the aorta or the left ventricle. Routine neck 3D TOF-MRA was used for reference as a guide for the determination of the tagging area in the selective vessel tagging (Fig. 2).

Three-dimensional TOF-MRA images were acquired for a comparison with the 4D-MRA findings. Neck TOF-MRA images were also acquired as a routine screening

tool as well as a support tool for the vessel-selective tagging described above. The imaging parameters of the 3D head TOF-MRA were as follows: gradient echo sequence, TR 20 ms, TE 3.5 ms, FOV 200 mm, matrix 512×256 (512×512 reconstruction), slice thickness 1.2 mm (slice pitch 0.6 mm), 182 slices, flip angle 18°, scan time 4’41. The imaging parameters of the 3D neck TOF-MRA were as follows: gradient echo sequence, TR 18.9 ms, TE 3.5 ms, FOV 250 mm, matrix 256×164 (512×512 reconstruction), slice thickness 2.0 mm (slice pitch 1.0 mm), 225 slices, flip angle 20°, scan time 6’03.

DSA technique

Intra-arterial digital subtraction angiography (DSA) was performed with a biplane system (AXIOM Artis, Siemens Healthcare, Erlangen, Germany). A selective catheterization was performed into the right carotid artery, left carotid artery and the dominant side of the vertebral artery, respectively, using a femoral artery approach in all patients. The DSA imaging from each artery was obtained by two projections (frontal and lateral views) separately. For each projection, 6–8 mL of iodinated contrast material was injected at the rate of 6–7 mL/sec using a power injector. The frame rate was 350 ms between phases. Images were obtained with a 1024×1024 matrix and a 21.5-cm FOV.

Image analysis

First, in the series of 36 VS-4D-MRA images, we determined the accuracy of the vessel selectivity by assessing whether only the targeted vessels were depicted or not. Next, using the data obtained by TOF-MRA, NS-4D-MRA and VS-4D-MRA, these images were respectively and independently evaluated based on the following points: (1) the identification of the feeding arteries, (2) the identification of the drainer veins, and (3) the measurement of the nidus size. As an additional evaluation of the VS-4D-MRA only, if multiple feeding arteries were suspected, we also determined (4) the percentage of the blood flow amount of each feeding artery in the entire nidus. All image evaluations were performed by two board-certified neuroradiologists (rater 1 with 19 years' experience and rater 2 with 12 years' experience).

Vessel selectivity assessment

The accuracy of the vessel selectivity was evaluated based on the following grading system: grade 0, clearly depicting an un-tagged vessel; grade 1, partly depicted an un-tagged vessel, which influenced the imaging interpretation and diagnosis; grade 2, slightly depicting an un-tagged vessel with no influence on the diagnosis; and grade 3, complete selectivity was achieved.

The identification of the feeding artery and drainer vein

We evaluated the identification of the feeding artery by identifying all feeding arteries and the side from which these vessels were running. The segment division of the feeding artery was based on the right and left anterior cerebral artery (ACA), the middle cerebral artery (MCA), the posterior cerebral artery (PCA), the anterior choroidal artery (AChA), the cerebral artery (including the superior, anterior-inferior, and posterior-inferior cerebellar arteries), and others. The identification of the drainer vein was evaluated based on the detection of the drainer vein and its flow direction to the cortical or deep side, or both. The identification of feeding arteries and the identification of draining veins were performed by the same two raters respectively. Validation of the MR findings was performed based on DSA findings. The final diagnoses from DSA findings were determined by consensus reading by the two neuroradiologists, who were blinded to patient information including MR findings; this determination was performed 1.5 month after the assessment of 4D-MRA.

The evaluation of the nidus size

In the evaluation of the nidus size, the maximum diameter of the nidus in each AVM was measured independently by the two neuroradiologists using the DSA, TOF-MRA, NS-4D-MRA and VS-4D-MRA images, and then the mean value of the two neuroradiologists' data was used as the nidus size. In VS-4D-MRA, we used the

maximum intensity projection (MIP) of each vessel-selective image (three series of Rt IC, Lt IC and BVA).

The evaluation of the percentage of the blood flow of each feeding artery to the entire nidus

In the case of multi-feeders, the percentage of the blood flow amount of each feeding artery in the entire nidus was evaluated by estimating the percentage value (0%–100%) by the partially depicted nidus from each feeding artery compared to the entire nidus lesion (=100%). The entire nidus lesion was estimated by referring to the TOF-MRA images. This estimation was performed mainly based on the depicted nidus size of both anterior-posterior and lateral projections by DSA or VS-4D-MRA compared to the total nidus size by TOF-MRA; the degree of density/signal intensity of the depicted nidus compared to that of feeding artery was also used as additional information. Finally, the percentage value was carefully determined with visual estimation of these overall findings by each rater. Each depicted nidus from each feeder was evaluated independently in a blind fashion; this evaluation was conducted so that the sum of the percentage values of all feeders in one AVM did not necessarily reach 100%. The estimation to determine the each feeder's percentage was performed in both DSA and VS-4D-MRA. In this evaluation, the mean value from the two

neuroradiologists was calculated and used as each feeder's percentage value.

Statistical analysis

We determined the interobserver agreement between the two neuroradiologists for the NS-4D-MRA and the VS-4D-MRA with respect to all evaluations by calculating the intraclass correlation coefficient (ICC) (0–0.2 poor agreement, 0.21–0.4 moderate agreement, 0.41–0.6 adequate agreement, 0.61–0.8 good agreement, 0.81–1.0 excellent agreement). In addition, a paired t-test was performed for 1) the values of nidus size (TOF-MRA, NS-4D-MRA and VS-4D-MRA, respectively) and 2) each feeder's percentage contribution to the entire nidus (DSA and VS-4D-MRA, respectively) for the assessment of interobserver variability between the two raters. Before the paired t-test, all measured values were confirmed to have a normal distribution by the Shapiro-Wilk test.

We compared the diagnostic accuracy of the three techniques (TOF-MRA, NS-4D-MRA and VS-4D-MRA) for the determination of the feeding artery and the drainer vein, respectively, by the chi-square test with the Bonferroni correction of the p-value. In the measurement of nidus size, we used a one-way analysis of variance (ANOVA) to compare the three techniques, with Tukey's post hoc method.

Bland-Altman analysis was also performed for the assessment of inter-modality variability. For the evaluation of each feeder's percentage blood flow amount compared to the entire nidus lesion, the sum of the percentage of all feeding arteries in each AVM was obtained by both VS-4D-MRA and DSA, and then the 'error value' was estimated as follows. First, the value of [error] was obtained using [error] = [sum of the percentage of all feeders in one AVM] − 100. By calculating the square root of the squared [error] (= absolute value of [error]), this value was defined as the 'error value' in each patient. By using the Mann-Whitney U-test, we compared the error values between the VS-4D-MRA and the DSA. P-values <0.05 were considered significant. However, the p-value was adjusted to <0.016 (= 0.05/3) in the case of the chi-square test for the Bonferroni correction.

Results

In the acquisition, the imaging plane was located to cover the circle of Willis and associated main branches sufficiently in all patients. All scanning was successfully performed without any complication or problem. As an evaluation of inter-observer agreement, the ICCs are summarized in Table 1. In the assessment of interobserver variability, no significant difference was observed in any measured value between the

two raters (Table 2). Vessel selectivity was graded 3 in 30 (rater 1) and 32 (rater 2) territories, and graded 2 in six (rater 1) and four (rater 2) territories. No scanning influenced the diagnosis by the contamination of another untagged vessel flow.

In the determination of the feeding arteries, successful and failed detection of all feeding arteries were summarized in Table 3. The detectability provided by the VS-4D-MRA was significantly higher than that of the other two methods in both rater 1 and 2 ($p<0.016$). In the evaluations of drainer veins, successful and failed detection of the drainer were summarized in Table 4. The detectability of the drainer veins by TOF-MRA was significantly higher compared to the VS-4D-MRA in both rater 1 and 2 ($p<0.016$).

In the evaluation of nidus size, there was no significant difference between the 4 scans (TOF-MRA, NS-4D-MRA, VS-4D-MRA and DSA), as shown in Table 5. The result of the Bland-Altman analysis is presented in Fig. 3.

In the percentage of the blood flow amount of each feeding artery in the entire nidus, a multi-feeder AVM was revealed by DSA findings in eight of the 12 patients, but one of these eight patients had two feeders only from a single vessel side (feeders of the left MCA and the left AChA from the left IC), and thus this patient was excluded from the evaluation. The error value in DSA was 27.1 ± 5.7 and 7.1 ± 3.9 in the VS-4D-MRA

(significantly smaller in the VS-4D-MRA; $p<0.001$) (Fig. 4).

Case example for the detection of the feeding artery and for the evaluation of each feeder's percentage blood flow amount in the entire nidus are shown in Fig. 5.

Discussion

In the present study, the VS-4D-MRA of the right ICA, left ICA and VBA was successfully conducted by using a free labeling slab. In several patients, the targeted selective vessel was not fully divided and there was a slight contamination of unselective vessels; however, serious contamination that affected the diagnostic performance was not observed. The detectability of the feeding arteries in the intracranial AVMs by VS-4D-MRA was confirmed; the diagnostic accuracy of VS-4D-MRA was superior to those of conventional TOF-MRA and NS-4D-MRA in detecting the feeding arteries. In addition, the results of our evaluation of the percentage of blood flow amount of each feeding artery in the entire nidus suggested that the blood flow amount estimation by DSA was probably an overestimation compared to the evaluation by VS-4D-MRA. A very limited number of studies assessing patients with intracranial AVM using 4D-MRA have been reported (11–13), and only one recent study that examined VS-4D-MRA in AVM patients can be found (15); however, in that study

the VS-4D-MRA was performed in two cases of AVM only for the illustration of this technique as case examples, and the clinical utility was not assessed. In contrast, the present study revealed the diagnostic utility of VS-4D-MRA and its advantage compared to the conventional technique of TOF-MRA and NS-4D-MRA.

In the results of the detectability of feeding artery, detectability by NS-4D-MRA was slightly higher than that of TOF-MRA, although a significant difference was not observed; this might be due to the small sample size in the current study. We suspect that the flow dynamic data of the timing of the visualization of the feeding artery to the nidus was helpful for the determination of each feeder, whereas TOF-MRA provided only static data, and thus such a diagnosis with the help of dynamic flow data cannot be achieved (12). However, in several of our cases, both TOF-MRA and NS-4D-MRA missed the accurate feeding artery that was running from an unexpected direction, such as the opposite-side arterial territory, because the visibility of all other arteries makes it difficult to find the true feeding artery from among the many visualized arteries. In such case, VS-4D-MRA will help detect the true feeding artery by visualizing only the targeted vessel. Moreover, 4D dynamic flow data also contribute to the diagnosis by adding the information of the dynamic flow to the nidus from each feeder, and the combination of such findings can provide more accurate

identification of the feeding arteries.

Regarding the assessment of the percentage of the blood flow amount of each feeding artery in the entire nidus, we observed that the sum of the percentage of each feeding artery tended to be far over 100% in the DSA findings. In contrast, the sum of the percentage of each feeding artery obtained using the VS-4D-MRA findings tended to be nearly 100% in most of the patients. We speculate that this interesting result occurred because VS-4D-MRA may have superior diagnostic power for the measurement of the involvement of each feeding artery to the nidus. DSA has often been performed using a power injector for the injection of the contrast agent, and the rate of injection is generally high, e.g., 5–6 ml/sec. Such a strong injection ("power injection") of contrast agent in DSA can generate a blood flow distribution that differs from the physiological condition, for instance due to reflux to other arterial territories (16). In assessing the percentage of blood flow amount in the entire nidus, we speculate such incorrect information due to a strong pressure injection of contrast agent will lead to an overestimation of depicted area because of the reflux of the area of the other arterial supply in the nidus. Unlike such an artificial blood flow by a power injector, arterial spin labeling uses arterial water alone as an endogenous tracer, and thus the complete physiological blood flow is reflected as dynamic flow imaging. We therefore

contend that VS-4D-MRA will reveal the true findings of the percentage of blood flow amount in each feeding artery in the entire nidus, which cannot be detected by the conventional DSA technique.

These advantages of VS-4D-MRA will be useful for the clinical assessment of AVM patients. For endovascular treatment or pre-surgical DSA as a detailed examination, advance information about feeding arteries will contribute to a rapid and smooth DSA procedure. In addition, the percentage of the blood flow amount of each feeder in the entire nidus will help in the determination of treatment priorities; with this information the operator can determine which artery should be treated first, second and next depending on the degree of involvement of each feeding artery with the nidus; moreover, it can be used for the estimation of the amount of embolic material to fill in the nidus sufficiently.

In contrast to these results, the detection of drainer veins by VS-4D-MRA was not superior to those of the conventional technique of TOF-MRA. In the vessel-selective technique, the total amount of labeled blood was smaller than that shown by the all-vessel tagging method and was considered not sufficient to detect the drainer veins with clear visualization. In particular, when labeled blood reaches the drainer vein, the inverted spin in arterial water will be mostly recovered and the labeling effect will

become very small, considering approx. 1.6 sec as the blood T1 value at 3T MR unit (17). In such a condition, it may be difficult to detect the drainer vein with sufficient visualization with only a small amount of labeled blood. The VS-4D-MRA technique can now be used for the arterial area and nidus evaluation but is not recommended to depict the drainer vein; this technique should be improved to address this disadvantage.

The present study has several limitations. First, the patient number was very small and the study was performed at a single institution. Although our findings provided information about the usefulness of vessel-selective 4D-MRA for the detection of feeding arteries and each feeder's blood flow contribution to the entire nidus even in such small number of patients, further analysis with larger patient number will be necessary to demonstrate the clinical superiority of the 4D-MRA technique. Second, the validation of the percentage of each feeder's blood flow amount in the entire nidus was difficult and probably not possible with any existing procedure. Thus, our statements about the present findings in this matter are only speculative.

In conclusion, the VS-4D-MRA technique was useful for the evaluation of intracranial AVMs by detecting the feeding arteries and for the estimation of the detailed information about the nidus. These findings indicate that the VS-4D-MRA technique

will be a helpful tool to obtain additional information in the assessment of AVM patients.

References

1. Hernesniemi JA, Dashti R, Juvela S, Vaart K, Niemela M, Laakso A. Natural history of brain arteriovenous malformations: a long-term follow-up study of risk of hemorrhage in 238 patients. Neurosurg 2008;63(5):823-829; discussion 829-831.
2. Spetzler RF, Martin NA. A proposed grading system for arteriovenous malformations. J Neurosurg 1986;65(4):476-483.
3. Duran M, Schoenberg SO, Yuh WT, Knopp MV, van Kaick G, Essig M. Cerebral arteriovenous malformations: morphologic evaluation by ultrashort 3D gadolinium-enhanced MR angiography. Eur Radiol 2002;12(12):2957-2964.
4. Hadizadeh DR, von Falkenhausen M, Gieseke J, et al. Cerebral arteriovenous malformation: Spetzler-Martin classification at subsecond-temporal-resolution four-dimensional MR angiography compared with that at DSA. Radiology 2008;246(1):205-213.
5. Soderman M, Andersson T, Karlsson B, Wallace MC, Edner G. Management of patients with brain arteriovenous malformations. Eur J Radiol. 2003;46(3):195-205.
6. Eddleman CS, Jeong HJ, Hurley MC, et al. 4D radial acquisition

contrast-enhanced MR angiography and intracranial arteriovenous malformations: quickly approaching digital subtraction angiography. Stroke 2009;40(8):2749-2753.

7. Willinsky RA, Taylor SM, TerBrugge K, Farb RI, Tomlinson G, Montanera W. Neurologic complications of cerebral angiography: prospective analysis of 2,899 procedures and review of the literature. Radiology 2003;227(2):522-528.

8. Marchal G, Bosmans H, Van Fraeyenhoven L, et al. Intracranial vascular lesions: optimization and clinical evaluation of three-dimensional time-of-flight MR angiography. Radiology 1990;175(2):443-448.

9. Petkova M, Gauvrit JY, Trystram D, et al. Three-dimensional dynamic time-resolved contrast-enhanced MRA using parallel imaging and a variable rate k-space sampling strategy in intracranial arteriovenous malformations. J Magn Reson Imaging 2009;29(1):7-12.

10. Taschner CA, Gieseke J, Le Thuc V, et al. Intracranial arteriovenous malformation: time-resolved contrast-enhanced MR angiography with combination of parallel imaging, keyhole acquisition, and k-space sampling techniques at 1.5 T. Radiology 2008;246(3):871-879.

11. Xu J, Shi D, Chen C, et al. Noncontrast-enhanced four-dimensional MR

angiography for the evaluation of cerebral arteriovenous malformation: a preliminary trial. J Magn Reson Imaging 2011;34(5):1199-1205.

12. Yu S, Yan L, Yao Y, et al. Noncontrast dynamic MRA in intracranial arteriovenous malformation (AVM), comparison with time of flight (TOF) and digital subtraction angiography (DSA). Magn Reson Imaging 2012;30(6):869-877.

13. Raoult H, Bannier E, Robert B, Barillot C, Schmitt P, Gauvrit JY. Time-resolved spin-labeled MR angiography for the depiction of cerebral arteriovenous malformations: a comparison of techniques. Radiology 2014;271(2):524-533.

14. Nakamura M, Yoneyama M, Tabuchi T, et al. Vessel-selective, non-contrast enhanced, time-resolved MR angiography with vessel-selective arterial spin labeling technique (CINEMA-SELECT) in intracranial arteries. Radiol Phys Technol 2013;6(2):327-334.

15. Jensen-Kondering U, Lindner T, van Osch MJ, Rohr A, Jansen O, Helle M. Superselective pseudo-continuous arterial spin labeling angiography. Eur J Radiol. 2015;84(9):1758-1767.

16. Hughes DG1, Patel U, Forbes WS, Jones AP. Comparison of hand injection with mechanical injection for digital subtraction selective cerebral angiography. Br J

Radiol. 1994;67(800):786-9

17. Lu H, Clingman C, Golay X, van Zijl PC. Determining the longitudinal relaxation time (T1) of blood at 3.0 Tesla. Magn Reson Med. 2004;52(3):679-682.

Table Captions and Figure Legends

Table 1. Intraclass correlation coefficient (ICC) between two neuroradiologists

	ICC between the two neuroradiologists
Accuracy in vessel selectivity	
vessel-selective 4D-MRA	0.93 (0.87, 0.97)
Idenfication of feeding artery	
all-vessel 4D-MRA	0.877 (0.56, 0.96)
vessel-selective 4D-MRA	0.92 (0.75, 0.98)
Idenfication of drainer vein	
vessel-selective 4D-MRA	0.81 (0.36, 0.95)
all-vessel 4D-MRA	0.72 (0.29, 0.91)
Measurement of the nidus size	
vessel-selective 4D-MRA	0.91 (0.72, 0.95)
all-vessel 4D-MRA	0.84 (0.64, 0.93)
Estimation in the percentage of the blood flow amount in each feeder	
vessel-selective 4D-MRA	0.74 (0.46, 0.95)

Footnote: Data are value of ICC. Data in parentheses are 95% confidence intervals.

Table 2. Interobserver variability in measurement of nidus size and percentage value for each feeder between the two neuroradiologists

	Rater 1	Rater 2	p value
Nidus size (mm)			
DSA	36.5±12.4	37.1±14.7	0.91
TOF-MRA	35.0±11.5	36.1±13.4	0.83
NS-4D-MRA	35.2±11.5	34.3±11.9	0.86
VS-4D-MRA	36.4±12.3	32.5±11.6	0.43
Percentage value in each feeder (%)			
DSA	52.1±21.1	51.2±24.1	0.91
VS-4D-MRA	41.4±20.1	42.1±21.2	0.93

Footnote: NS-4D-MRA, non-vessel-selective 4D-MRA; VS-4D-MRA, vessel-selective 4D-MRA.

Table 3. Detail of evaluation in feeding artery

Feeding artery detected by each technique (Rater 1)

Pt. No.	Confirmed feeders by DSA	TOF-MRA	NS-4D-MRA	VS-4D-MRA
1	Lt ACA, Rt. PCA	Rt. ACA, Rt PCA	Rt. ACA, Rt PCA	Lt ACA, Rt. PCA
2	Rt. ACA, Rt. PCA	Rt. ACA, Rt. PCA	Rt. ACA, Rt. PCA	Rt. ACA, Rt. PCA
3	Lt. PCA	Lt. PCA	Lt. PCA	Lt. PCA
4	Lt. ACA, Rt. MCA, Rt. PCA	Lt. ACA, Rt. MCA, Rt. PCA	Lt. ACA, Rt. MCA, Rt. PCA	Lt. ACA, Rt. MCA, Rt. PCA
5	Rt. ACA, Rt. MCA, Rt. PCA	Rt. ACA, Rt. MCA, Rt. PCA	Rt. ACA, Rt. MCA, Rt. PCA	Rt. ACA, Rt. MCA, Rt. PCA
6	Lt. MCA	Lt. MCA	Lt. MCA	Lt. MCA
7	Rt. ACA, Lt. ACA	Lt. ACA	Lt. ACA	Rt. ACA, Lt. ACA
8	Rt. SCA	Rt. SCA, Rt. PCA	Rt. SCA	Rt. SCA
9	Lt. MCA	Lt. MCA, Lt. PCA	Lt. MCA, Lt. PCA	Lt. MCA
10	Lt. MCA, Lt. AChA	Lt. MCA, Lt. AChA	Lt. MCA, Lt. AChA	Lt. MCA, Lt. AChA
11	Rt. ACA, Rt. MCA, Rt. PCA	Rt. ACA, Rt. MCA, Rt. PCA	Rt. ACA, Rt. MCA, Rt. PCA	Rt. ACA, Rt. MCA, Rt. PCA
12	Rt. ACA, Rt. MCA	Rt. ACA, Lt. ACA, Rt. MCA	Rt. ACA, Lt. ACA, Rt. MCA	Rt. ACA, Rt. MCA
	Sensitivity	0.91	0.91	1
	Specificity	0.96	0.96	1
	Positive predictive value	0.84	0.88	1
	Negative predictive value	0.98	0.97	1
	Accuracy	0.95	0.95	1
Cases corresponding to DSA		7 in 12	8 in 12	12 in 12

Feeding artery detected by each technique (Rater 2)

Pt. No.	Confirmed feeders by DSA	TOF-MRA	NS-4D-MRA	VS-4D-MRA
1	Lt ACA, Rt. PCA	Rt PCA	Rt. ACA, Rt PCA	Rt. PCA
2	Rt. ACA, Rt. PCA	Rt. ACA, Rt. PCA	Rt. ACA, Rt. PCA	Rt. ACA, Rt. PCA

3	Lt. PCA	Lt. PCA	Lt. PCA	Lt. PCA
4	Lt. ACA, Rt. MCA, Rt. PCA	Lt. ACA, Rt. MCA, Rt. PCA	Lt. ACA, Rt. MCA, Rt. PCA	Lt. ACA, Rt. MCA, Rt. PCA
5	Rt. ACA, Rt. MCA, Rt. PCA	Rt. ACA, Rt. MCA, Rt. PCA	Rt. ACA, Rt. MCA, Rt. PCA	Rt. ACA, Rt. MCA, Rt. PCA
6	Lt. MCA	Lt. MCA	Lt. MCA	Lt. MCA
7	Rt. ACA, Lt. ACA	Lt. ACA	Lt. ACA	Rt. ACA, Lt. ACA
8	Rt. SCA	Rt. SCA, Rt. PCA	Rt. SCA, Rt. PCA	Rt. SCA
9	Lt. MCA	Lt. AchA, Lt. MCA, Lt. PCA	Lt. AchA, Lt. MCA, Lt. PCA	Lt. MCA
10	Lt. MCA, Lt. AChA	Lt. MCA	Lt. MCA, Lt. AChA	Lt. MCA, Lt. AChA
11	Rt. ACA, Rt. MCA, Rt. PCA	Rt. ACA, Rt. MCA, Rt. PCA	Rt. ACA, Rt. MCA, Rt. PCA	Rt. ACA, Rt. MCA, Rt. PCA
12	Rt. ACA, Rt. MCA	Rt. ACA, Lt. ACA, Rt. MCA	Rt. ACA, Lt. ACA, Rt. MCA	Rt. ACA, Rt. MCA
	Sensitivity	0.87	0.91	0.96
	Specificity	0.95	0.95	1
	Positive predictive value	0.8	0.81	1
	Negative predictive value	0.97	0.98	0.99
	Accuracy	0.94	0.95	0.99
Cases corresponding to DSA		6 in 12	7 in 12	11 in 12

Footnote: ACA, anterior cerebral artery; AChA, anterior choroidal artery; Lt., left; MCA, middle cerebral artery; NS-4D-MRA, non-vessel-selective 4D-MRA; PCA, posterior cerebral artery ; Rt., right; SCA, superior cerebellar artery; VS-4D-MRA, vessel-selective 4D-MRA.

Table 4. Detail of evaluation in drainer vein

Drainer vein detected by each technique (Rater 1)

Pt. No.	Confirmed drainers by DSA	TOF-MRA	NS-4D-MRA	VS-4D-MRA
1	deep vein	cortical and deep vein	cortical vein	no vein detected
2	cortical and deep vein	cortical and deep vein	cortical vein	cortical vein
3	cortical and deep vein	cortical and deep vein	cortical vein	cortical vein
4	cortical vein	cortical vein	cortical vein	cortical vein
5	cortical vein	cortical vein	cortical vein	cortical vein
6	cortical vein	cortical vein	cortical vein	cortical vein
7	cortical vein	cortical vein	cortical vein	cortical vein
8	cortical and deep vein	cortical and deep vein	cortical and deep vein	cortical and deep vein
9	deep vein	deep vein	deep vein	deep vein
10	cortical and deep vein	deep vein	deep vein	no vein detected
11	cortical vein	cortical vein	cortical vein	cortical vein
12	cortical and deep vein	cortical and deep vein	cortical and deep vein	cortical vein
	Sensitivity	0.94	0.76	0.65
	Specificity	0.86	0.86	1
	Positive predictive value	0.94	0.93	1
	Negative predictive value	0.86	0.6	0.54
	Accuracy	0.92	0.79	0.75
Cases corresponding to DSA		10 in 12	8 in 12	7 in 12

Drainer vein detected by each technique (Rater 2)

Pt. No.	Confirmed drainers by DSA	TOF-MRA	NS-4D-MRA	VS-4D-MRA

1	deep vein	cortical and deep vein	no vein detected	no vein detected
2	cortical and deep vein	cortical and deep vein	cortical and deep vein	no vein detected
3	cortical and deep vein	cortical and deep vein	cortical vein	cortical vein
4	cortical vein	cortical vein	cortical vein	cortical vein
5	cortical vein	cortical vein	cortical vein	cortical vein
6	cortical vein	cortical vein	cortical vein	cortical vein
7	cortical vein	cortical vein	cortical vein	cortical vein
8	cortical and deep vein	cortical vein	cortical vein	cortical vein
9	deep vein	deep vein	deep vein	deep vein
10	cortical and deep vein	cortical and deep vein	cortical and deep vein	deep vein
11	cortical vein	cortical vein	cortical vein	cortical vein
12	cortical and deep vein	cortical and deep vein	cortical and deep vein	cortical vein
	Sensitivity	0.94	0.82	0.59
	Specificity	0.86	1	1
	Positive predictive value	0.94	1	1
	Negative predictive value	0.86	0.7	0.5
	Accuracy	0.92	0.88	0.71
Cases corresponding to DSA		10 in 12	9 in 12	6 in 12

Footnote: NS-4D-MRA, non-vessel-selective 4D-MRA; VS-4D-MRA, vessel-selective 4D-MRA.

Table 5. Detail of the measurement of nidus size

	DSA	TOF-MRA	NS-4D-MRA	VS-4D-MRA	p value
Nidus size (mm)	36.8±13.1	35.5±12.1	34.7±11.3	34.4±11.8	0.82

Footnote: NS-4D-MRA, non-vessel-selective 4D-MRA; VS-4D-MRA, vessel-selective 4D-MRA.

Figure Legends

Fig. 1. Schema of the 4D-MRA sequence. The acquisition of labeled and control images was performed within one sequence. In both the labeled and control images, after each labeling pulse or control pulse, multi-phase images were acquired using Look-Locker sampling with TFEPI readout. After the acquisition, by subtracting the labeled image from the control image and providing the maximum intensity projection (MIP), the 4D-MRA image was generated (*bottom row*).

Fig. 2. Details of the vessel-selective tagging. Examples of selective tagging placed on TOF-MRA in the right common carotid artery (a: MIP image, b: axial source image), left common carotid artery (c: MIP image, d: axial source image) and bilateral vertebral artery (e: MIP image, f: axial source image). To obtain the vessel-selective tagging, the labeling slab was carefully placed so that each main trunk was divided and any other trunk was avoided in the labeling slab anatomically by referring to the axial, coronal and sagittal MIP images and the raw MRA image of neck (a–f, red area).

Fig. 3. Bland-Altman plot graph of the nidus size differences.

Compared to the nidus size measured by DSA, no large shift of mean bias was observed in TOF-MRA (a), non-vessel-selective 4D-MRA (b) or vessel-selective 4D-MRA (c).

Fig. 4. Error values of DSA and vessel-selective 4D-MRA (VS-4D-MRA) for the assessment of the percentage blood flow amount of each feeder in the entire nidus. The error value of the VS-4D-MRA (7.1 ± 3.9) was significantly smaller than that of DSA (27.1 ± 5.7) (*; significant difference).

Fig. 5. Images of a left frontal lobe AVM in a 30-year-old male. From TOF-MRA (a), the lesion of the nidus was observed in the left frontal lobe (a: arrow). In the TOF-MRA and non-vessel-selective 4D-MRA (NS-4D-MRA) (b), it was difficult to determine whether the right ACA was related to the nidus as a feeding artery. In contrast, with the vessel-selective 4D-MRA (VS-4D-MRA) with Rt. IC-selective tagging (c), it was easy to determine the relation of the Rt. ACA to the nidus as a feeding artery (c: arrow). The amount of arterial supply to the nidus was observed a little inVS-4D-MRA. However, the findings of right carotid angiography (CAG) indicated a greater degree of involvement with the nidus (d: arrow). The VS-4D-MRA with Lt. IC-selective tagging (e) revealed the blood supply to most of the nidus and well corresponded to the

left-CAG findings (f). Much overlapped area was observed between the nidus depicted by right-CAG and left-CAG, whereas there was a little overlapped area between Rt. and Lt. IC-selective tagging in VS-4D-MRA: we suspect that this finding was overestimated because of the power injection of contrast agent in DSA by refluxing the other arterial territory in the nidus.

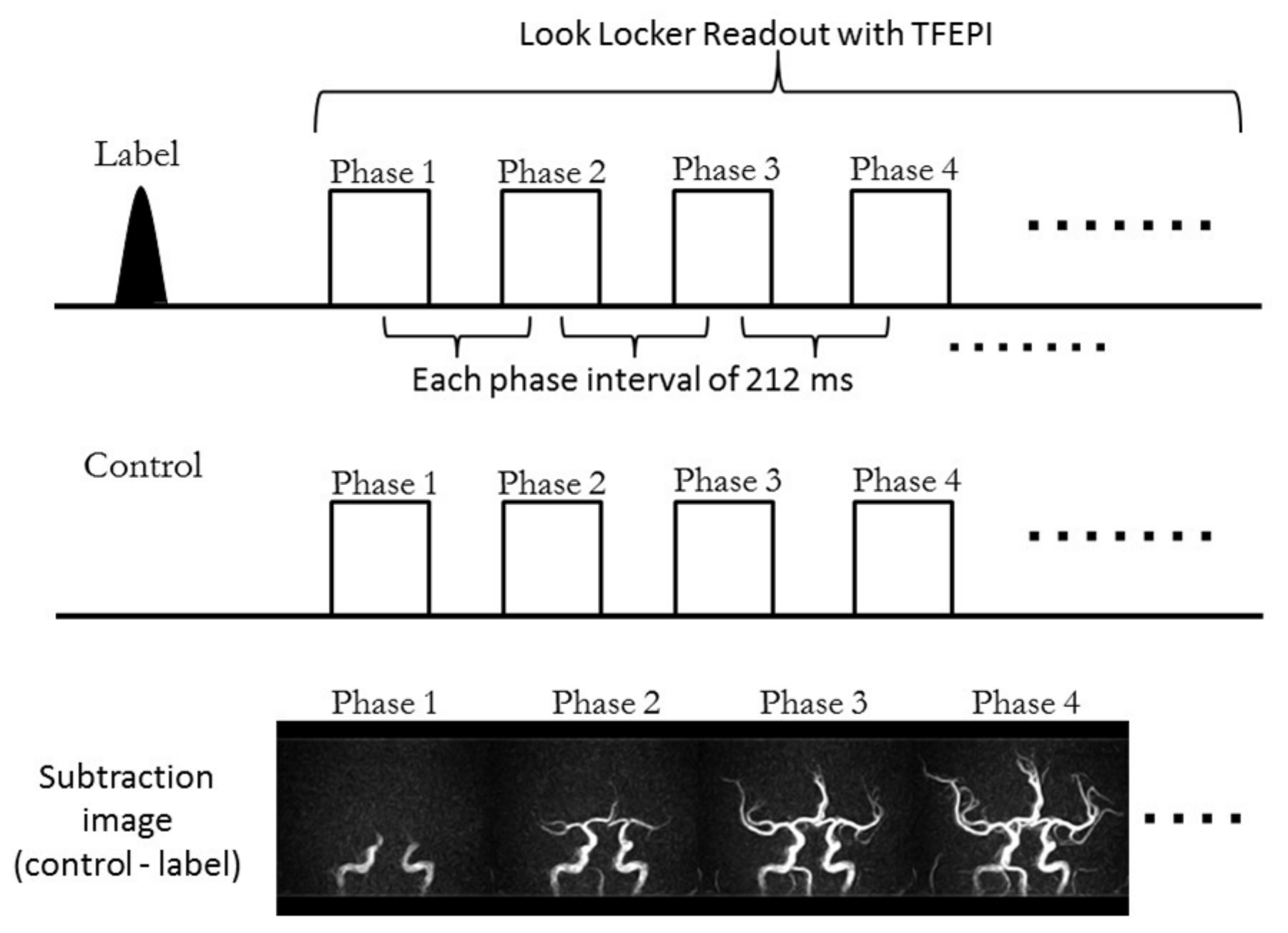
Look Locker Readout with TFEPI
Label
Phase 1
Phase 2
Phase 3
Phase 4
Each phase interval of 212 ms
Control
Phase 1
Phase 2
Phase 3
Phase 4
Phase 1
Phase 2
Phase 3
Phase 4
Subtraction image (control - label)

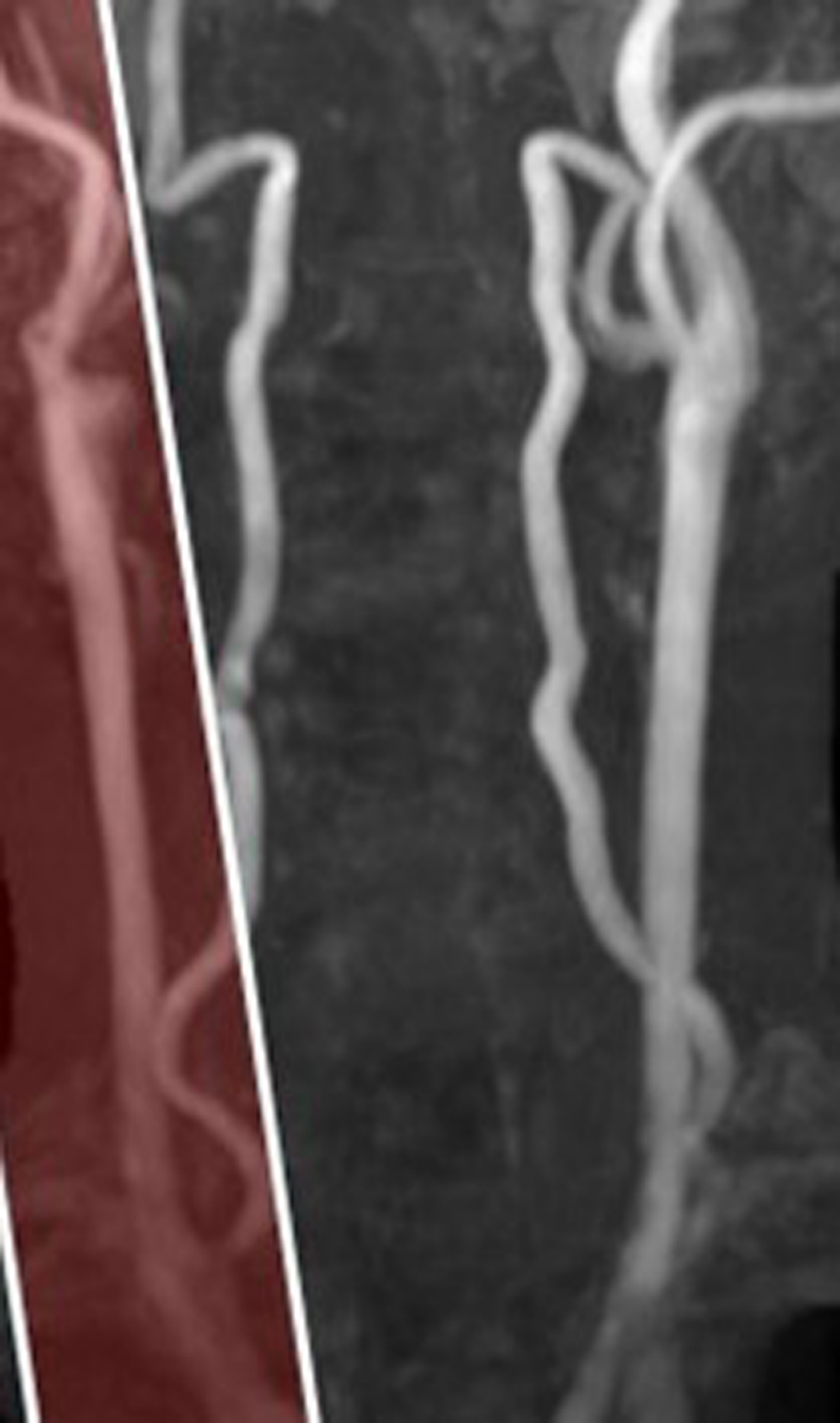

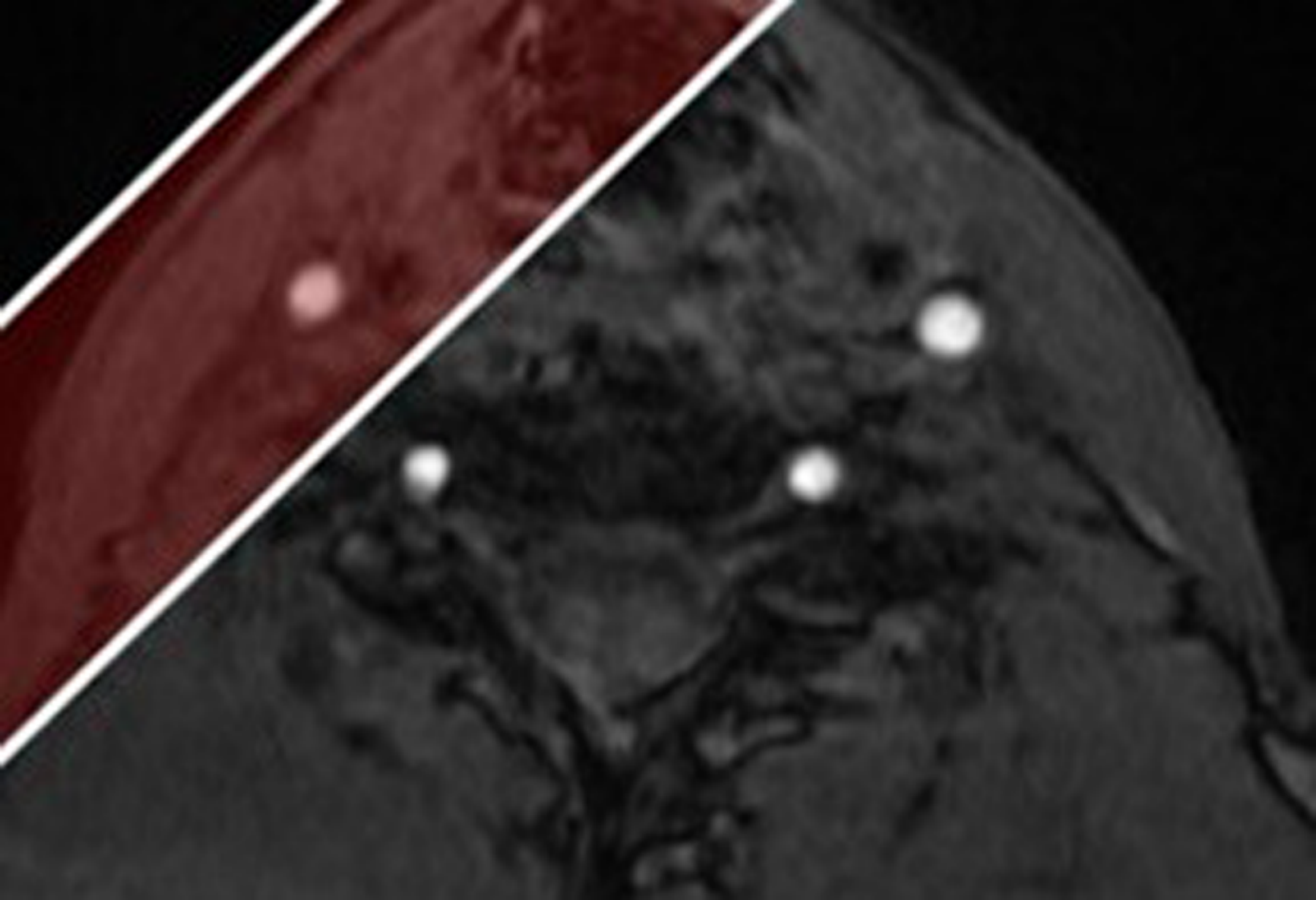

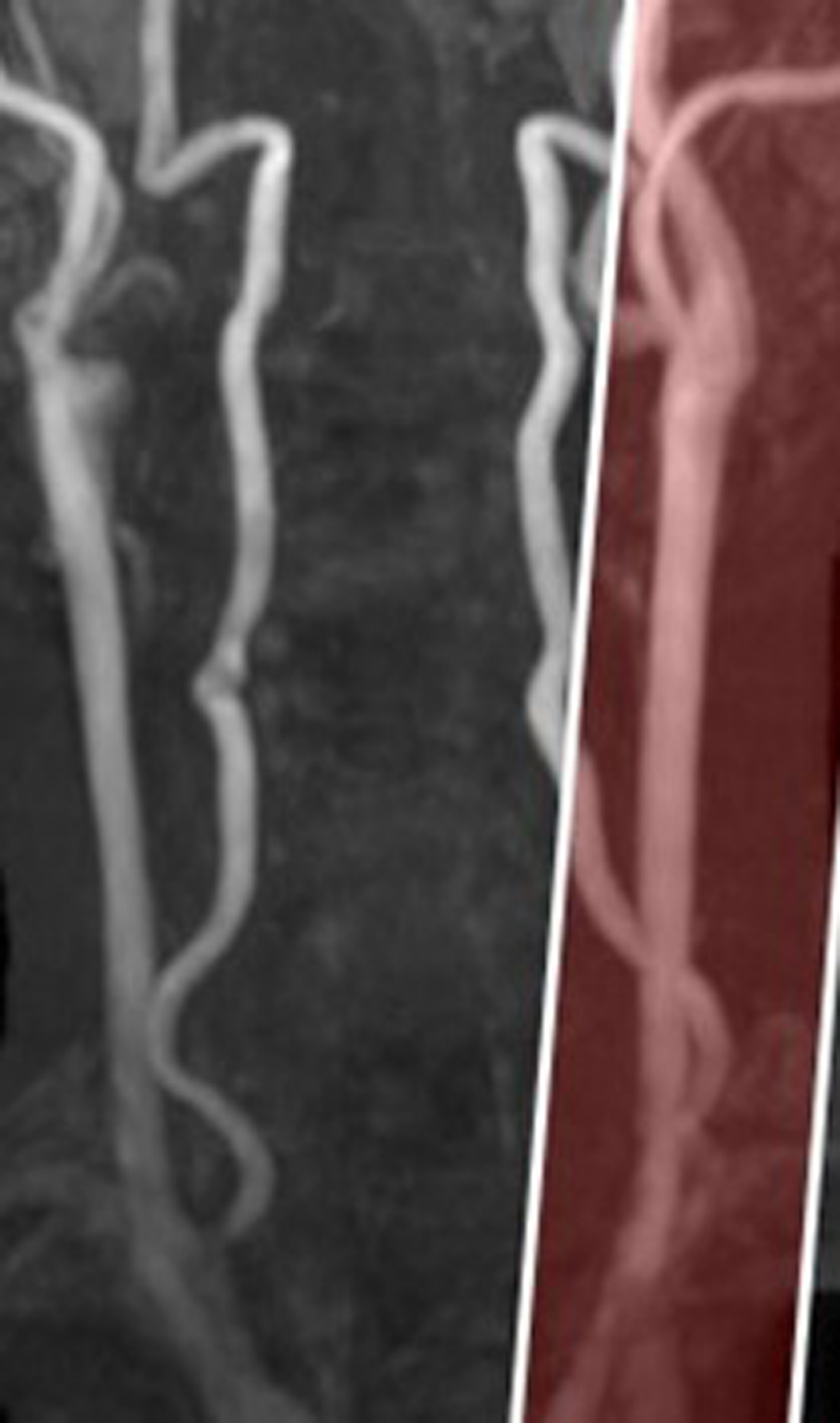

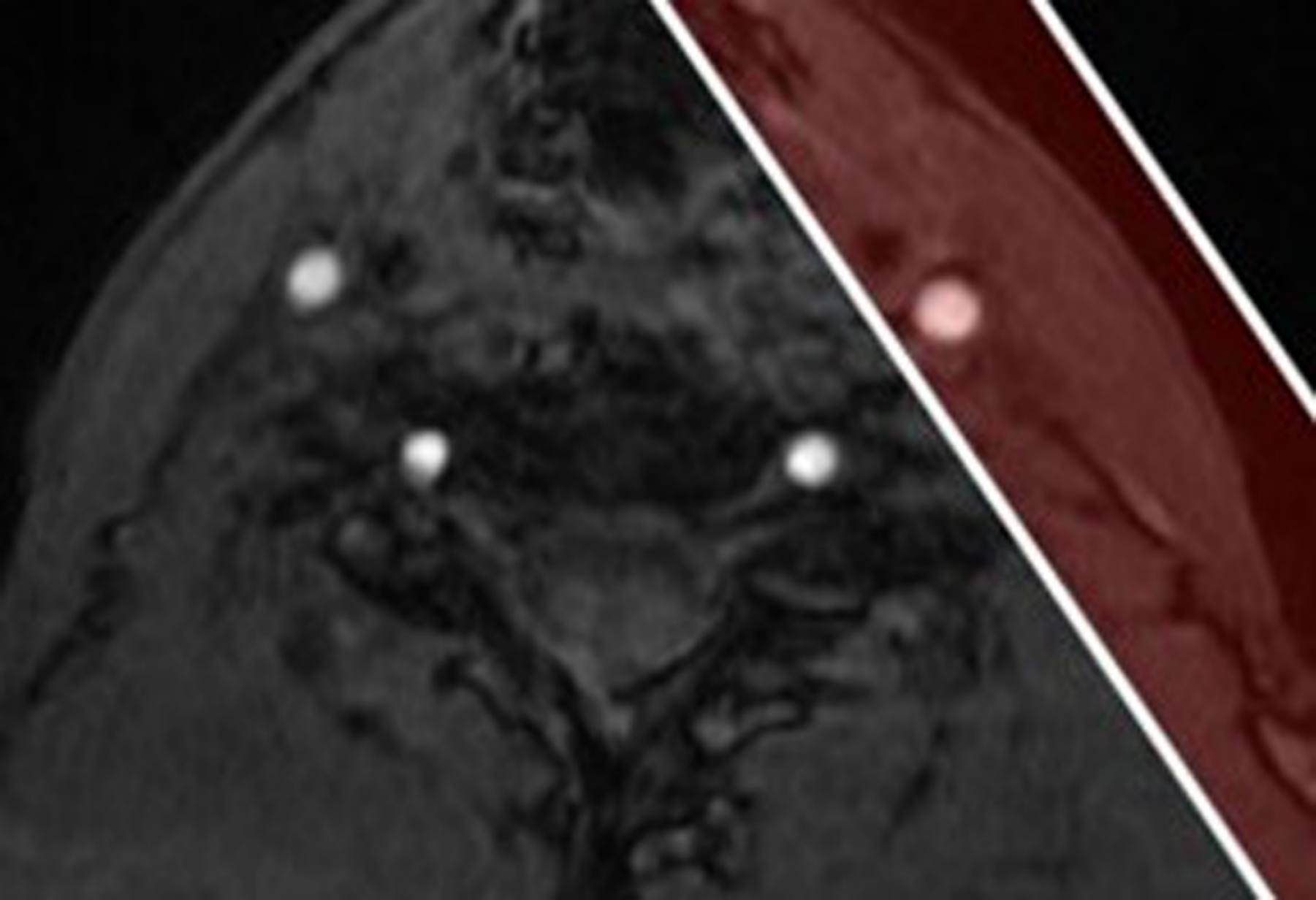

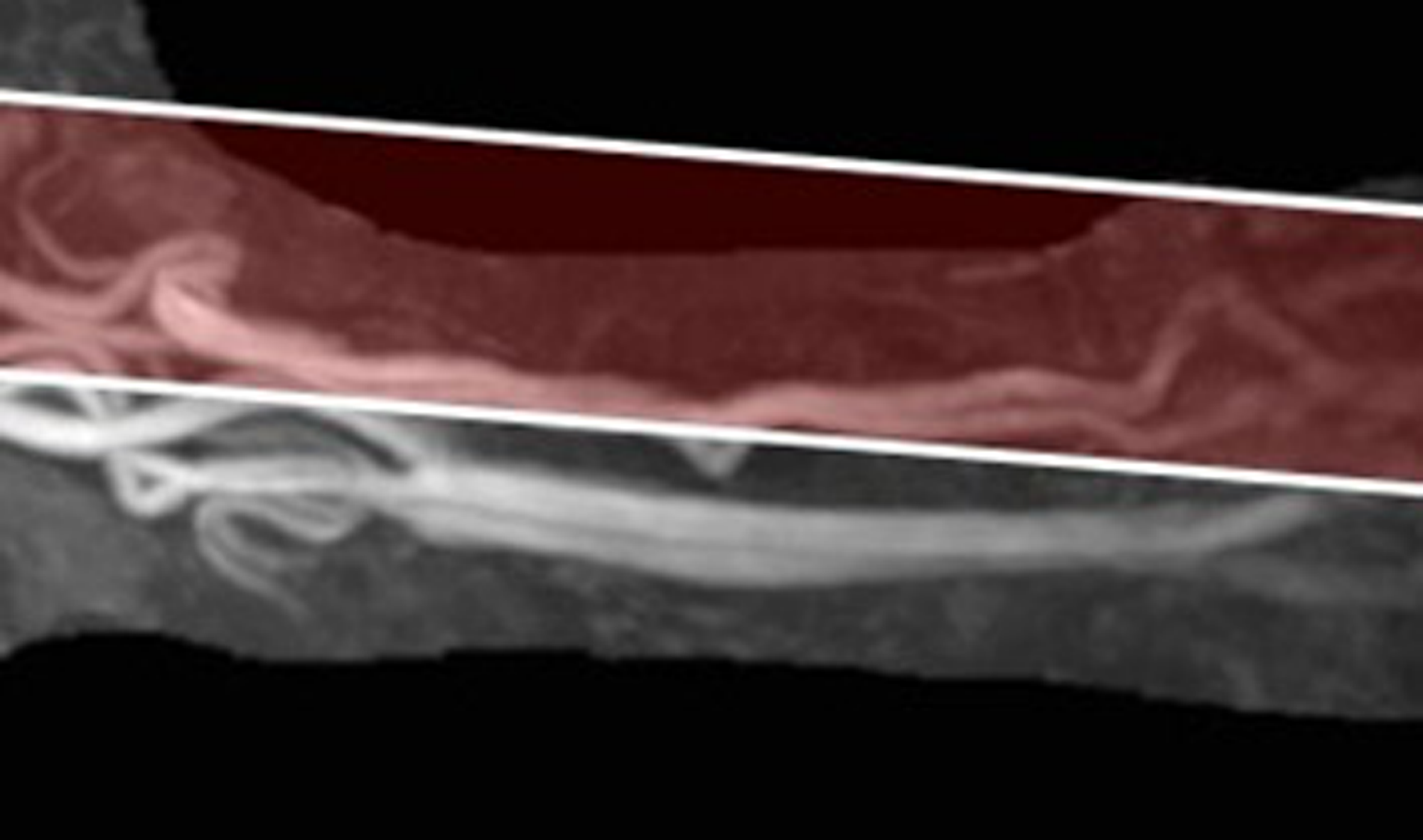

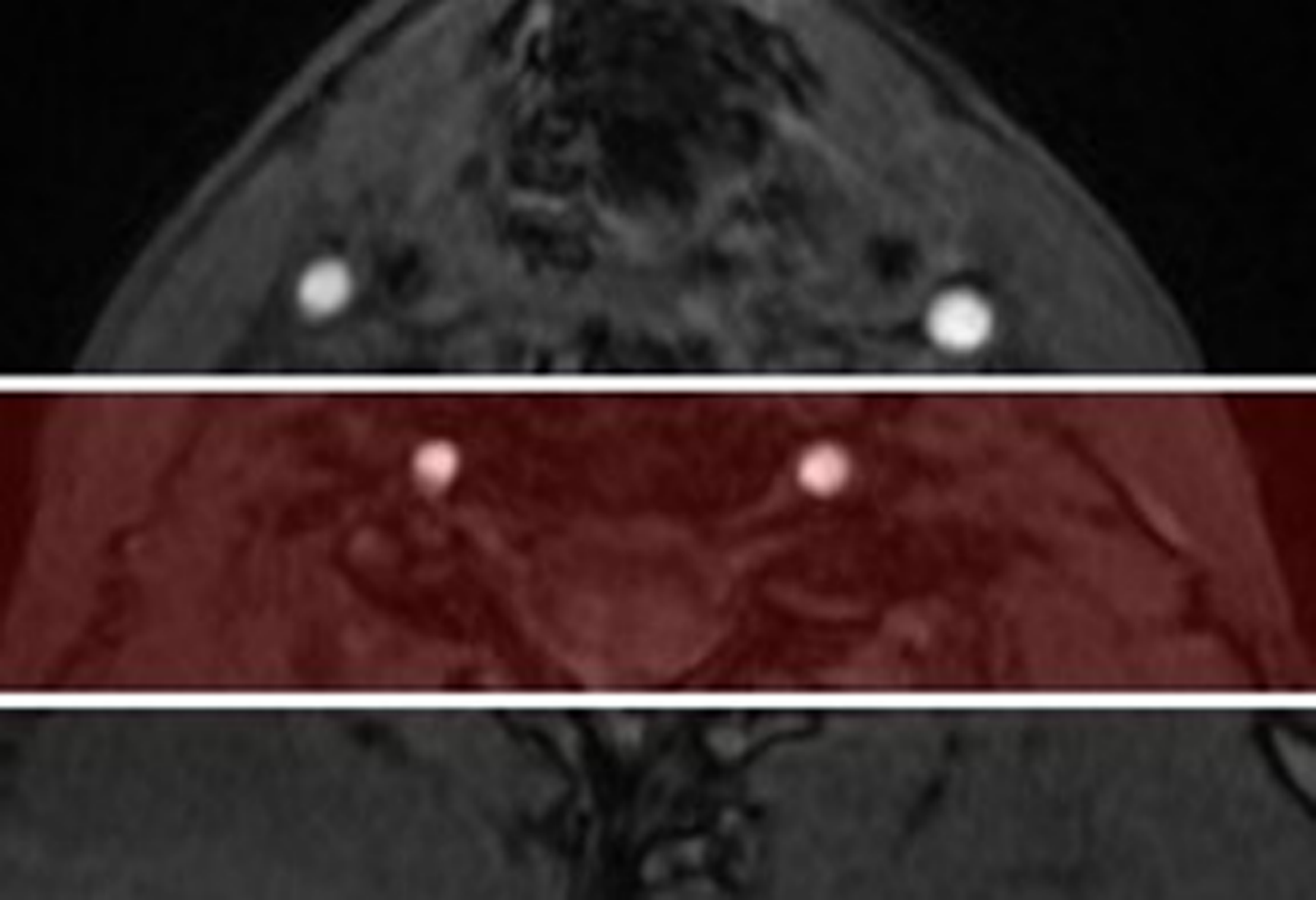

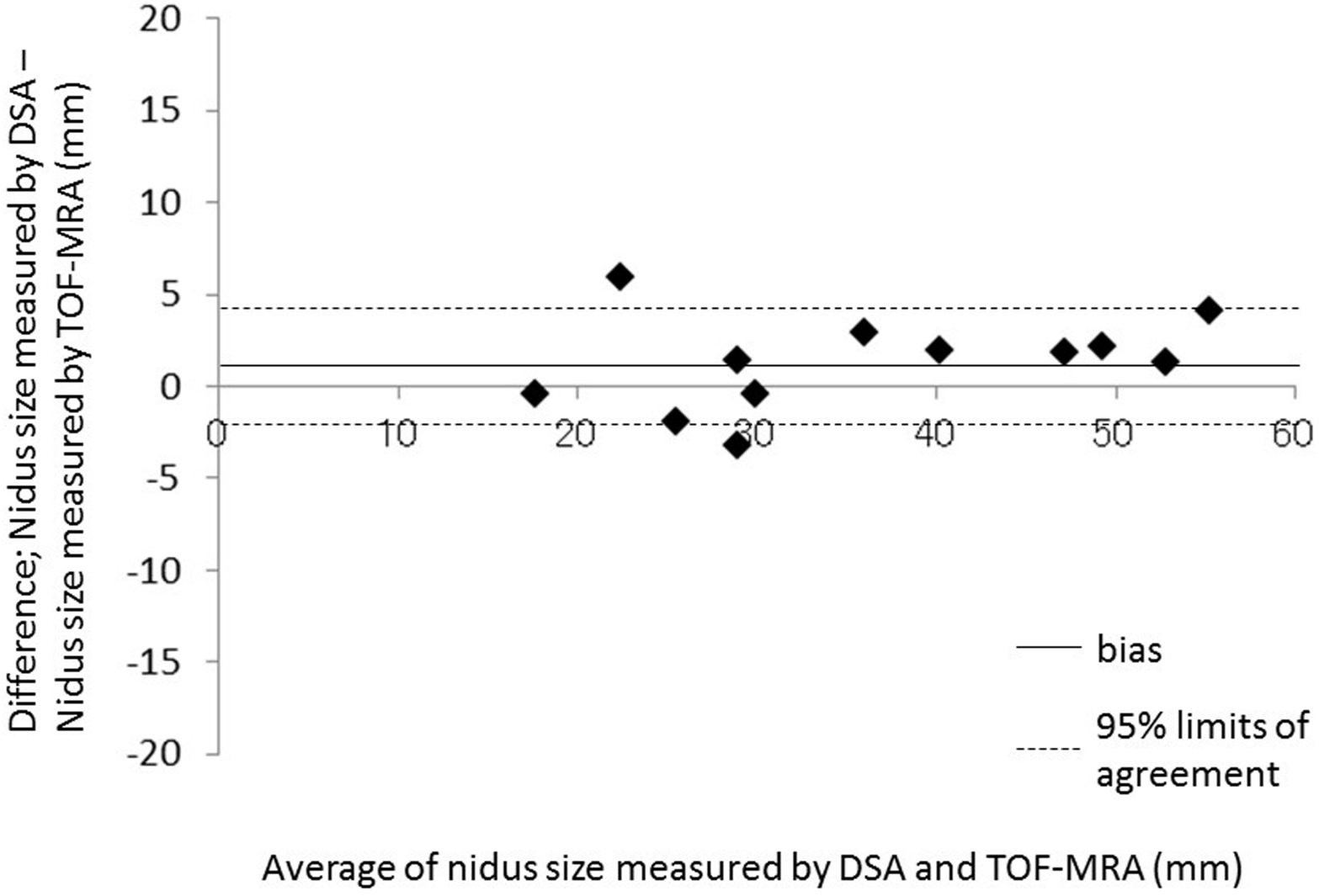
Difference; Nidus size measured by DSA – Nidus size measured by TOF-MRA (mm)
20
15
10
5
0
-5
-10
-15
-20
0
10
20
30
40
50
60
bias
95% limits of agreement
Average of nidus size measured by DSA and TOF-MRA (mm)

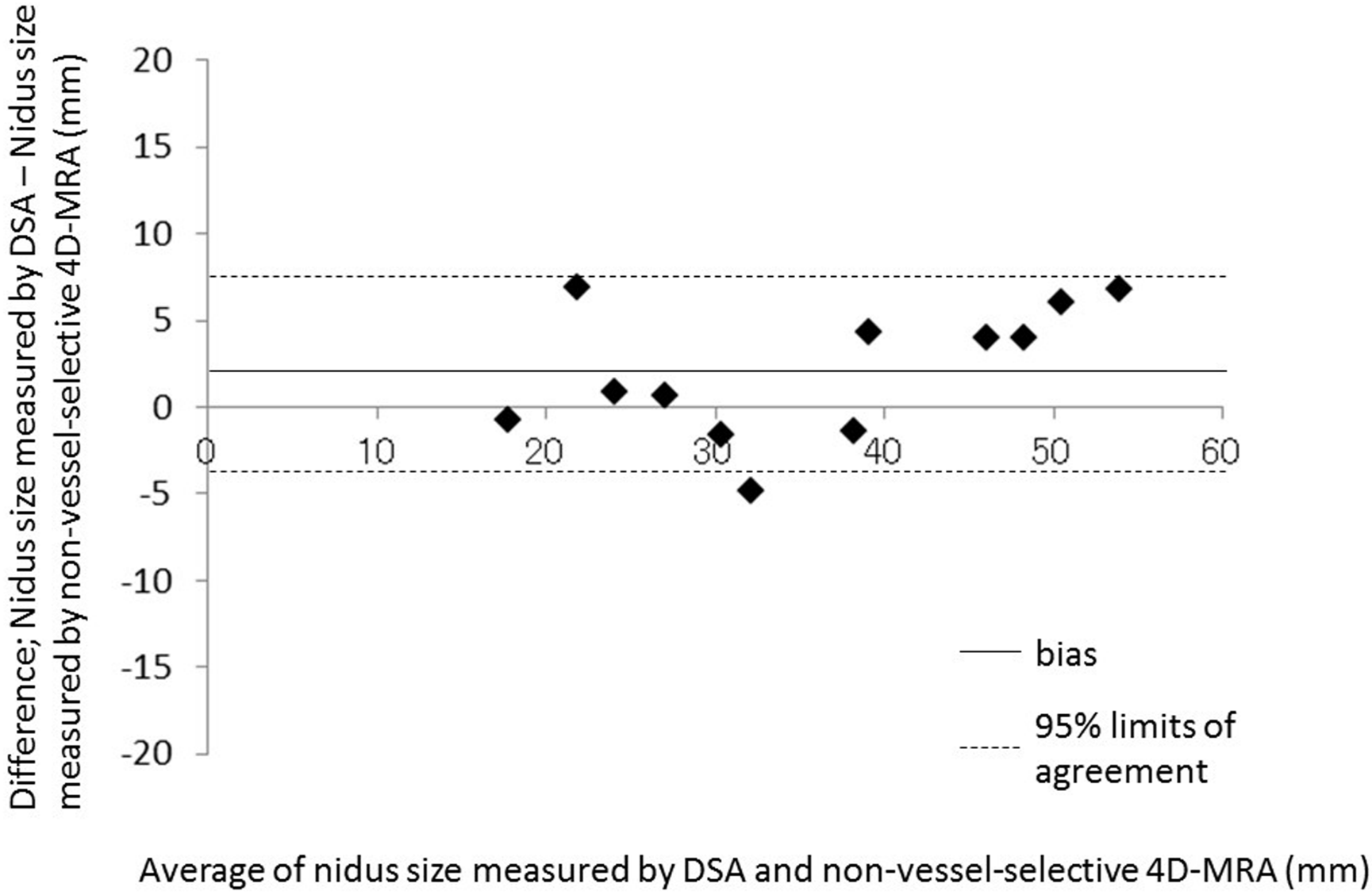
Difference; Nidus size measured by DSA – Nidus size measured by non-vessel-selective 4D-MRA (mm)
20
15
10
5
0
-5
-10
-15
-20
0
10
20
30
40
50
60
bias
95% limits of agreement
Average of nidus size measured by DSA and non-vessel-selective 4D-MRA (mm)

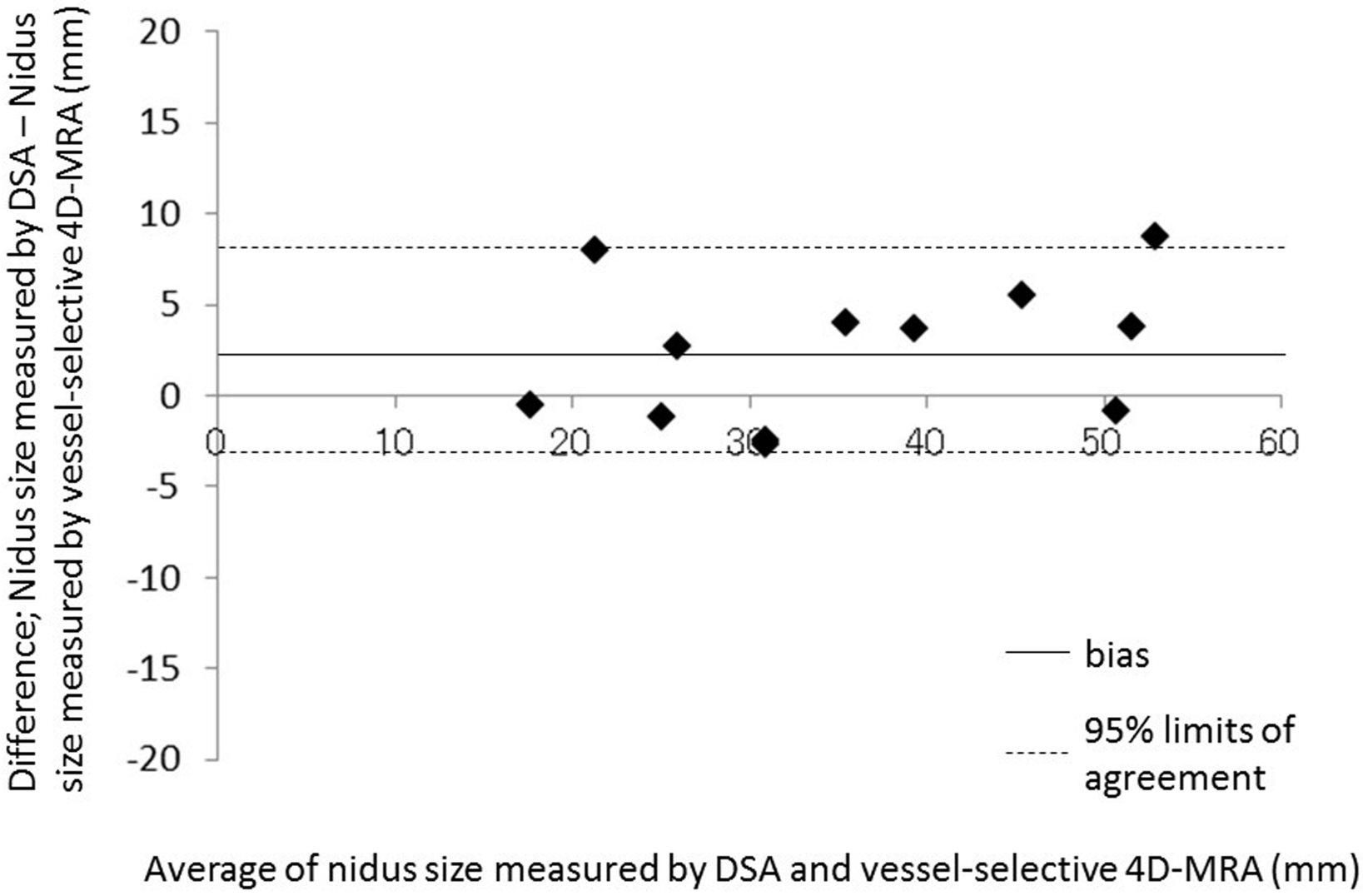
Difference; Nidus size measured by DSA – Nidus size measured by vessel-selective 4D-MRA (mm)
20
15
10
5
0
-5
-10
-15
-20
0
10
20
30
40
50
60
bias
95% limits of agreement
Average of nidus size measured by DSA and vessel-selective 4D-MRA (mm)

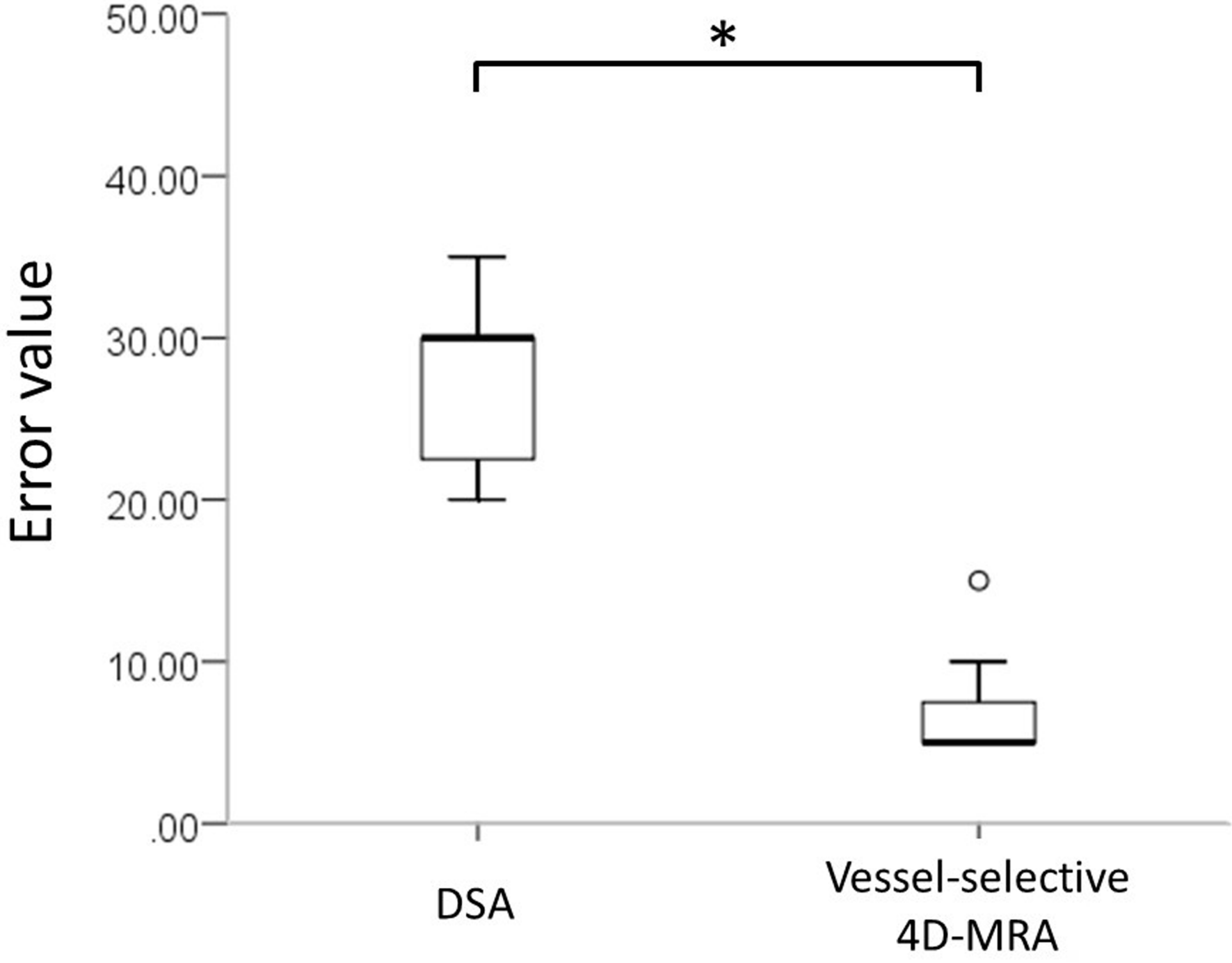
50.00
40.00
30.00
20.00
10.00
.00
Error value
*
DSA
Vessel-selective
4D-MRA